Influence of time-delay feedback on extreme events in a forced Liénard system

R. Suresh* and V. K. Chandrasekar†
Centre for Nonlinear Science and Engineering, School of Electrical and Electronics Engineering, SASTRA Deemed University, Thanjavur 613 401, India

(Received 20 June 2018; published 9 November 2018)

A periodically forced Liénard system is capable of generating frequent large-amplitude chaotic bursts for a range of system and external forcing parameter values which are known as mixed mode oscillations. Particularly, if these large chaotic bursts occur infrequently and randomly, then they are characterized as extreme events. We present a numerical study of the effect of self-time-delay feedback on these extreme events in this system and interestingly find that extreme events can be completely eliminated from the system dynamics, even for smaller values of delay feedback strength. We show here that the number of extreme events is reduced, and the probability of the occurrence of high-amplitude events is transformed from a long-tailed statistics to the localized structure, as a function of the feedback strength corroborates our results. Further, we show that the autonomous Liénard system loses its conservative nature when delay feedback is added and only a dissipative nature remains in the entire phase space, which is the underlying mechanism behind the elimination of such large events. Further, we have revealed a type of delay-induced damping behavior, named *anomalous damping*, in which the amplitude of the oscillations suddenly vanishes when the total energy of the system becomes zero.

DOI: 10.1103/PhysRevE.98.052211

I. INTRODUCTION

The occurrence of sudden, rare, and recurrent high- or low-amplitude oscillations (events) are inevitable in natural and human-made systems [1]. Usually, the time evolution of the system observables oscillate or fluctuate between a well-defined threshold level (derived from their long-time average). In spite of that, at certain conditions, there exist a large-amplitude oscillation along with small-amplitude oscillations that differ significantly (2 to 4 times larger than usual) from ordinary events, which are called mixed mode oscillations (MMOs). Specifically, if these oscillations occurred occasionally and randomly, then they are distinguished as extreme events which appeared in diverse areas of science. In particular, the generation of rogue waves in oceanography and optical systems [2–7]; the occurrence of floods, droughts, rainfall, earthquakes, and volcanic eruptions in geophysics [8,9]; jamming in computer and transportation networks [10–12]; development of epileptic seizures in the human brain [13,14]; stock market crashes in economics [15]; harmful algal blooms in marine life ecosystems [16,17]; and large-scale power blackouts in electrical power supply networks [18] are few of the examples.

In natural systems, due to the scarcity of observation data available for the corresponding rare events, the detailed study of such events and their mechanism of generation and prediction is difficult. In order to overcome these problems, extreme events with similar statistical properties have already been studied and identified in theoretical models and in simple laboratory-based experiments. For instance, it has been shown that extreme events exhibited in excitable and oscillatory systems like the FitzHugh-Nagumo model, the Ginzburg-Landau model, the nonlinear Schrödinger equation, pulse coupled oscillatory systems, a Liénard-type system, semiconductor and optically injected laser model systems, nonlinear electronic circuits, etc., and different emerging mechanisms have been discussed and reported in the literature [19–27]. In some of the systems mentioned above, the occurrence of extreme events is an inherent property of the systems regarding to the system parameters and in other cases it is occurred due to the external perturbations. In general, it has been examined that there are three main types of mechanisms that trigger extreme events in certain classes of dynamical systems [28]. In the first type, extreme events appear as chaotic bursts in dynamical systems where the motion is separated into distinct time scales (slow-fast dynamical systems) [19–21,29,30]. Another mechanism which induces extreme events is the occurrence of chaotic bursting through homoclinic and heteroclinic orbits [31,32]. Finally, the noise-induced transition is another important class of extreme event mechanism occurred in dynamical systems where the equilibrium points are stable in the absence of noise, and there is a transition from one equilibrium to other in the presence of noise [33–35]. Besides, several other mechanisms, like a sudden expansion of a chaotic attractor via internal or external crisis, time-delay feedback induced extreme events, and weak successive backscattering-induced extreme events, have also been identified and reported in recent times [23,36–39]. Another important aspect of the extreme event is the controlling mechanism. Even though controlling such events is difficult in many natural systems, it is entirely possible and highly desired but remains a challenge in artificial systems, such as power grid networks, optical systems, traffic networks, the human brain, etc. Especially, in lasers, high-intensity pulses

*suresh@eee.sastra.edu
†chandrasekar@eee.sastra.edu

capable of producing catastrophic optical damage have been observed [7,40]. Very recently, the controlling mechanism of the extreme events in dynamical systems has been attempted and demonstrated in the literature [12,16,24,41–43]. However, only a limited number of studies are available and systematic research involving control of extreme events is still missing.

Recently, it was reported that a forced Liénard-type system is capable of producing large-amplitude events along with the small oscillations under the influence of an external periodic force for a wide range of parameter values [22,23]. In particular, in Ref. [23], the authors presented the numerical and experimental results of the occurrence of extreme events and demonstrated that such events occur via two processes, internal crisis and intermittency. Also, the mechanism for the emergence of extreme events has been discussed. It has already been proved that time-delay feedback can give rise to several interesting novel dynamical behaviors [44–47].

Motivated by the above studies, in this paper, we study the dynamics of the autonomous Liénard system with self-time-delay feedback and with external periodic forcing. We give analytical reasoning with supporting numerical evidence for the emergence and mechanism of large-amplitude events in this system. The autonomous Liénard system has an interesting property where it acts as a conservative or dissipative system depending on the choice of system parameters and initial conditions. We will show that under the influence of external periodic forcing the dissipative and conservative regions of the system collide at certain times due to the movement of equilibrium points and when the chaotic trajectory crosses the saddle point during these times, repelled by the saddle point, and make a large excursions in the phase space to produce high-amplitude oscillations. Although the Liénard system exhibit MMOs for wide parameter range, in this paper, we mainly concentrate on the dynamics of extreme events in the presence of time-delay feedback.

We have identified that when increasing the strength of delay feedback, the number of extreme events are drastically reduced and eliminated from the system even for minimal values of feedback strength. We show that while increasing the feedback strength, the size of the large events remains the same but the number of extreme events are reduced. In contrast, in other recent findings [37,38], the authors demonstrated that the size and number of extreme events had been increased when increasing the delay feedback in a diode laser system with phase-conjugate feedback. Also, we have verified that the conservative nature of the autonomous Liénard system is disappeared when adding the time-delayed feedback and only dissipative nature remains in the entire phase space. Hence, the trajectories starting from these regions damp slowly to reach the stable fixed point. Further, we have revealed a type of damping behavior in which amplitude of the oscillations suddenly vanishes (with respect to the time) when the total energy of the system becomes zero. We call this critical transition phenomenon as anomalous damping bahavior which is similar like tipping points or regime shifts where one dynamical state is suddenly changed into another state in parametric space which occurred in many physical, ecological, and biological systems and in climate dynamics [48–50].

The remaining paper is organized as follows: In Sec. II, we will give a brief introduction to the system we have chosen for our study. We will explain the dynamics of an autonomous Liénard system in Sec. III A and explore the effect of external periodic forcing in Sec. III B. Influence of delay feedback on extreme events is demonstrated in Sec. IV. Mechanism of controlling extreme events is discussed in Sec. IV A and the existence of anomalous damping behavior is described in Sec. IV B. Finally, in Sec. V, we summarize our results with conclusions.

II. SYSTEM DESCRIPTION

The system which we have chosen for our study is a Liénard-type oscillator with external periodic forcing and self-time-delayed feedback. The mathematical form of the equation is represented by

$$\dot{x} = y, \tag{1a}$$

$$\dot{y} = -\alpha x y + \gamma x - \beta x^3 + F\sin(\Omega t) + \varepsilon x_\tau. \tag{1b}$$

Here α is the nonlinear damping parameter, γ is related to the internal frequency of the system, β indicates the strength of nonlinearity, and F and Ω are the amplitude and frequency of the periodic external force, respectively; $x_\tau = x(t-\tau)$ is the delayed variable of $x(t)$ with time delay τ and ε is the strength of delay feedback. The autonomous Liénard-type equation has received much attention from both the mathematics and physics perspectives. For example, this equation governs spherically symmetric expansion and collapse of a relatively gravitating mass [51]. It occurs in the study of a spherical gas cloud acting under the mutual interaction of its molecules and subject to the laws of thermodynamics [52,53] and it also used in the modeling of the fusion of pellets [54]. The nonlinear type of damping has been found in many chemically relevant kinetic equations [55]. This equation can also be thought of as a one-dimensional counterpart of the boson "gauge-theory" equations introduced by Yang and Mills [56]. Furthermore, the forced Liénard system with time-delayed feedback has been used to model the optoelectronic oscillator dynamical systems [57,58]. Other than that, for the past several years the invariance and integrability properties of the equation have been studied in detail [59–63]. Further, we also emphasize here that the autonomous Liénard system (1) is an example of the reversible system under the transformation

$$S : (x, y, t) \rightarrowtail (-x, y, -t). \tag{2}$$

Reversible dynamical systems have been shown to play an essential role in Hamiltonian and non-Hamiltonian dynamics [64–68]. This equation admits a nonstandard conservative Hamiltonian nature and interesting dynamical properties [69]. Specifically, for a particular parameter choice ($\beta = \frac{\alpha}{9}$), the system admits isochronous oscillation property [62] and exhibiting (parity-time ($\mathcal{PT}$) symmetry and broken $\mathcal{PT}$-symmetric nature [70]. The coupled version of the system shows twofold $\mathcal{PT}$ symmetry in nonlinearly damped dynamical systems [71]. Further, the existence of different types of chimera-like dynamical states has been observed in a network of globally coupled Liénard system [72].

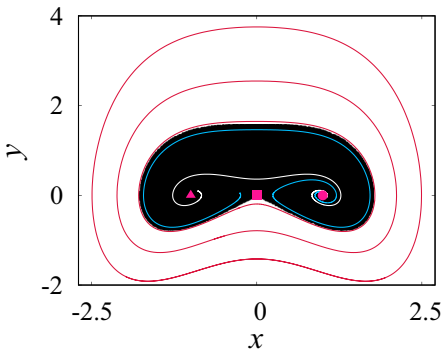

FIG. 1. Phase portrait of the autonomous Liénard system [Eq. (1)] with $F = 0$ and $\tau = 0$. The filled circle, square, and triangle represent the stable focus, saddle origin, and unstable focus equilibrium points, respectively, for the parameter values $\alpha = 0.45$, $\gamma = 0.5$, and $\beta = 0.5$. The black region indicates the basin of attraction for the dissipative nature and the white region represents the basin of attraction for the conservative nature. Distinct color lines are plotted for different initial conditions corroborated the dissipative and conservative natures of the system. See text for explanation.

In the following sections, we will study the dynamics of a Liénard-type system with three different cases: (i) dynamics of autonomous Liénard system, (ii) effect of external periodic forcing, and (iii) influence of self-time-delay feedback.

III. RESULTS AND DISCUSSION

A. Dynamics of autonomous Liénard system

In this section, we have presented the results of the dynamical study of Eq. (1) without external forcing and time delay. For our numerical simulations, we have fixed the values of system parameters $\gamma = 0.5$ and $\beta = 0.5$ throughout the manuscript. For $F = 0$ and $\tau = 0$, with the above chosen parameter values and for $\alpha > 0$ the system has three equilibrium points: a stable focus at $(x, y) = (1, 0)$, a saddle point at (0,0), and an unstable focus at $(-1, 0)$, which are clearly depicted in Fig. 1 as a filled circle, square, and triangle, respectively. Here the stable focus point at (1,0) is linearly stable and nonlinearly unstable. That is, the trajectories dissipate and approach to the stable focus only if we choose the initial conditions within some region in the phase space. Otherwise, the orbits exhibit limit-cycle oscillations. Hence, based on the initial conditions the system has either a dissipative or conservative nature. In Fig. 1 the black region represents the basin of attraction of the dissipative nature. The border which separates the black and white regions is known as the homoclinic orbit. Initial conditions started within this homoclinic orbit converge to the stable focus at (1,0). For instance, the white and light blue/gray trajectories in Fig. 1 started near the unstable and saddle points, respectively, traveled in the phase space and ended up at the stable focus. However, if we choose the initial conditions in the white region (denotes the basin of attraction for the conservative nature), the system has an infinite number of coexisting neutrally stable periodic orbits which oscillate with respect to the saddle origin. In Fig. 1, we have illustrated three such orbits [red (black) lines] plotted for three different initial conditions. Hence, the autonomous Liénard system exhibits the coexistence of conservative and dissipative behavior. We also note here that these orbits are nonisochronous (here, the frequency of oscillation is proportional to the amplitude) periodic orbits.

As we mentioned earlier, the autonomous Liénard system is an example of a reversible dynamical system. The coexistence of dissipative and conservative nature in the reversible dynamical systems have already been reported in the literature [64–68]. In particular, in Ref. [65], Politi *et al*. have demonstrated the possibilities of the coexistence of both conservative and dissipative behaviors in non-Hamiltonian systems. They have also shown that the physical system they considered displays symmetry-breaking bifurcations and the phase-space structure changes from conservative to dissipative nature either in continuous or discontinuous fashion above the critical value of the system parameters.

The dynamical system which we have considered here clearly demonstrate the coexistence of conservative and dissipative nature. In the autonomous Liénard system, if $\gamma < 0$, then the system exhibits a conservative nature in the whole phase space. Nevertheless, for $\gamma \geqslant 0$ and $8\beta > \alpha^2$, the system shows the coexisting conservative and dissipative nature, even if the system admits Hamiltonian dynamics. The reason for the dual nature of the autonomous Liénard system can be explained by deriving the total energy of the system. The total energy of Eq. (1) without forcing and time-delay feedback terms can be written as

$$\widetilde{E} = \frac{1}{2}\left[y^2 + \frac{\alpha y}{2}\left(x^2 + \frac{\gamma}{\beta}\right) + \frac{\beta}{2}\left(x^2 + \frac{\gamma}{\beta}\right)^2\right] \times e^{\frac{\alpha}{\omega}\tan^{-1}\left[\frac{\alpha y + 2\beta\left(x^2+\frac{\gamma}{\beta}\right)}{2\omega y}\right]} - \left(\frac{\gamma^2}{4\beta}\right)e^{\frac{\alpha\pi}{2\omega}}, \tag{3}$$

where $\omega = (\frac{1}{2})\sqrt{8\beta - \alpha^2}$. If we substitute the initial conditions of the system variables (x, y) in Eq. (3), then for some initial conditions $\widetilde{E}$ has negative values and for other initial conditions it has positive values. The system exhibits dissipative dynamics if $\widetilde{E} < 0$, and when $\widetilde{E} > 0$ it displays a conservative nature. In particular, in the black region of Fig. 1, the total energy of the system has negative values and so the trajectories originated from this area have a dissipative nature and converge towards the stable focus when time persists. On the other hand, initial conditions chosen in the white region have a positive $\widetilde{E}$ value and hence the trajectories exhibit conservative nature with neutrally stable periodic orbits as depicted in Fig. 1.

In the next section, we will demonstrate the dynamical behavior of the Liénard system in the presence of external periodic force.

B. Dynamics of forced Liénard system

If we introduce a periodic external force with $F \neq 0$ in Eq. (1) without delay feedback ($\tau = 0$), then the symmetry of the system is broken. Hence the fixed points become asymmetric and they start moving along the x axis depending on the forcing amplitude. Due to this movement of fixed points, the dissipative and conservative regions of the system oscillate in terms of the forcing amplitude in the time domain.

As a result, the dissipative region is enhanced in the phase space. During this oscillatory motion of the fixed points when $F = F_c = \frac{2\gamma}{3}\sqrt{\frac{\gamma}{3\beta}} \approx 0.19245$ (for the chosen parameter values), the stability of the system is changed periodically. For instance, if $0 < F < F_c$ ($F_c < F < -F_c$), then the unstable (stable) focus and saddle equilibrium points move towards each other and for $F = F_c$ ($F = -F_c$) the two fixed points collide and disappeared via saddle-node bifurcation and only a stable (unstable) fixed point is feasible. Therefore, a three-fixed-point system is transformed into a single-fixed-point system and vice versa with respect to the time. With regard to the amplitude of the external periodic force, the system changes its stability when

$$t_k = \frac{2k\pi + \sin^{-1}\left(\frac{F_c}{F}\right)}{\Omega}, \tag{4a}$$

$$t_{2k} = \frac{(2k+1)\pi - \sin^{-1}\left(\frac{F_c}{F}\right)}{\Omega}, \tag{4b}$$

$$t_{3k} = \frac{(2k+1)\pi + \sin^{-1}\left(\frac{F_c}{F}\right)}{\Omega}, \tag{4c}$$

$$t_{4k} = \frac{2(k+1)\pi - \sin^{-1}\left(\frac{F_c}{F}\right)}{\Omega}, \tag{4d}$$

where $k = 0, 1, 2, \ldots$. For $t_{4k-1} < t < t_k$ and $t_{2k} < t < t_{3k}$ the system has three fixed points. On the other hand, the system has a single fixed point during $t_k < t < t_{2k}$ and $t_{3k} < t < t_{4k}$. This oscillation in fixed points is known as a stretching and folding property which leads to chaotic behavior if we choose the initial conditions in the dissipative region and for suitable values of F and Ω. The system shows chaotic behavior when it satisfies the condition

$$8\Omega \,\mathrm{sech}\left(\frac{\pi\Omega}{\sqrt{2}}\right) - \frac{\alpha}{F} \gtrapprox 0, \tag{5}$$

which was analytically derived from Melnikov's method [73] by considering the nonlinear damping (α) and forcing (F) terms in Eq. (1) as perturbation.

The dynamical nature of the forced Liénard system is studied and illustrated as a one-parameter bifurcation diagram in Fig. 2 as a function of the forcing frequency in the range of $\Omega \in (0.62, 0.78)$ with $F = 0.2$. This figure demonstrates the two distinct dynamical routes to the birth of chaotic dynamics when we increase or decrease the forcing frequency. If one looks at Fig. 2 from right to left by decreasing the forcing frequency, the periodic attractor bifurcates into a bounded chaotic attractor via period doubling bifurcation. The bounded chaotic orbit slowly expands in size with decreasing forcing frequency and at $\Omega \approx 0.7316$ it suddenly expanded into a large size attractor. This large size attractor continues to remain for further decreasing of forcing frequency, and at $\Omega \approx 0.64225$ the chaotic orbit suddenly bifurcates into a period-I attractor via intermittency route.

From this bifurcation diagram, it is evident that when varying the forcing frequency in the range of $\Omega \in (0.64225, 0.7316)$ the system exhibit MMOs in which large- and small-amplitude chaotic oscillations of different frequencies coexist. In other words, for these Ω values the system display small-amplitude bounded chaotic oscillations along

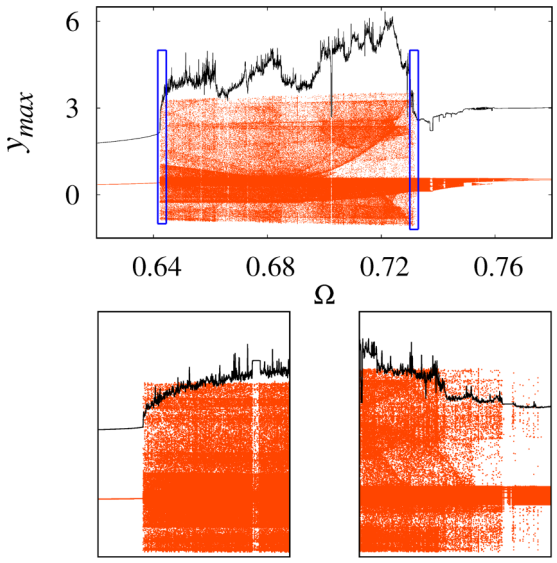

FIG. 2. One-parameter bifurcation diagram drawn using the maxima of the dynamical variable y of Eq. (1) with $F = 0.2$ and $\tau = 0$ illustrating the occurrence of distinct dynamical behaviors as a function of the external forcing frequency ($\Omega \in (0.62, 0.78)$). Other system parameters are fixed as given in Fig. 1. The black line indicates the H_s. The magnified regions of the figure are depicted in the bottom panel. For more details, see text.

with frequent intermittent large-amplitude chaotic bursting. Interestingly, for some range of Ω, these large-amplitude chaotic bursts occurred occasionally and randomly. These states have been separately characterized and reported as extreme events [23]. The temporal dynamics of the forced system showing the bounded chaos, MMOs, and extreme event dynamics for different values of forcing frequency (Ω) is explained in Appendix A. We wish to note here that the extreme events are also a type of MMOs but the rare occurrence of the large chaotic bursts distinguish it from the MMOs. In order to classify the extreme events from MMOs, we have numerically calculated $H_s = (\langle P_n \rangle + 8\sigma)$ with the temporal data of the y component (observation time of the data: 2×10^9 time units after leaving sufficient transient). Here $\langle P_n \rangle$ is the time-averaged peak value of the y component and σ is the standard deviation. For MMOs the average value of the large-amplitude peaks is very high and so H_s becomes larger than the peaks. On the other hand, during the existence of extreme events the large peaks exhibit occasionally. Hence, the average value of the peaks are higher than H_s. Therefore, amplitudes which are higher than H_s can be defined as extreme events. We have plotted H_s in Fig. 2, which is indicated as a black line along with the bifurcation diagram. We can see in the marked rectangle regions of Ω (enlarged and depicted in the bottom panel of Fig. 2) that the maxima of the y component are larger than H_s corroborate the occurrence of extreme events for these Ω ranges. In other regions of Ω, H_s is larger than the peaks corroborate the existence of MMOs. The mechanism for the emergence of MMOs and extreme events can be explained as follows: The autonomous Liénard system has dual nature of dissipative and conservative dynamics depending on the choice of initial

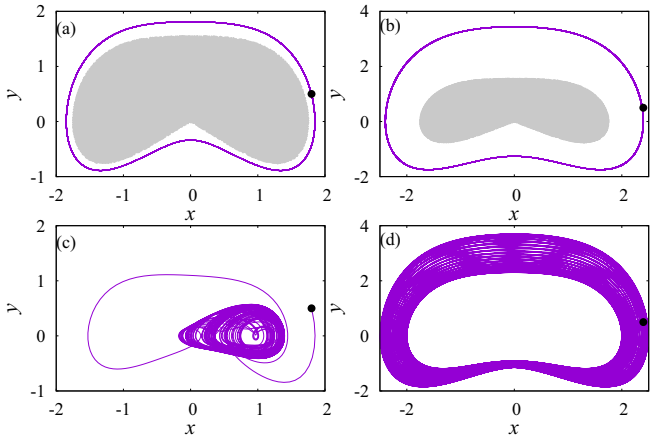

FIG. 3. [(a) and (b)] Phase portraits of the autonomous Liénard system depicted for two different initial conditions chosen near and away from the homoclinic orbit, respectively, shows the neutrally stable periodic orbits. The gray area indicates the dissipative region of the system and the chosen initial conditions are marked as filled circles. [(c) and (d)] The chaotic and quasiperiodic dynamics of the forced Liénard system evolved from the same initial conditions for $F = 0.2$ and $\Omega = 0.7314$ with the above chosen initial conditions.

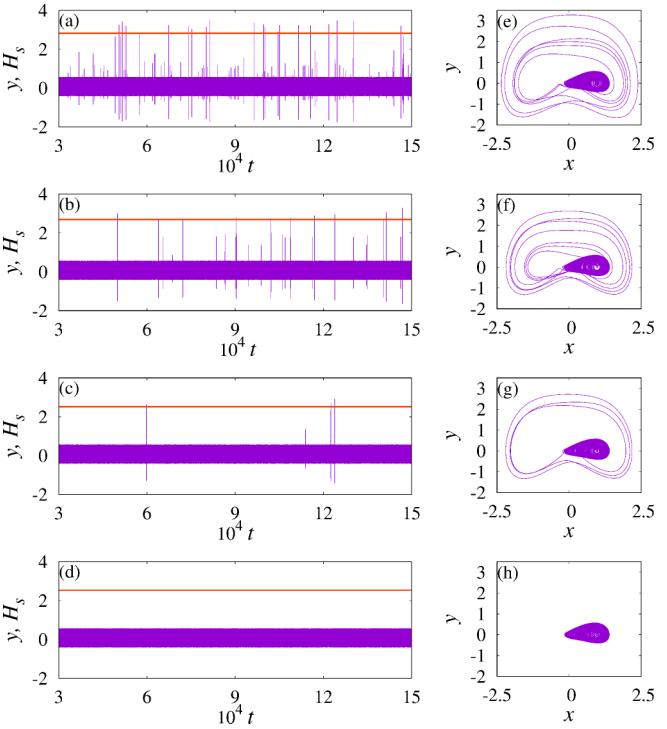

FIG. 4. [(a)–(d)] Temporal dynamics and [(e)–(h)] the corresponding phase-space diagrams of the forced Liénard system with $F = 0.2$, $\Omega = 0.7314$, $\tau = 0.1$ and for different values of the delay feedback strength (ε); [(a) and (e)] for $\varepsilon = 0.0$, [(b) and (f)] for $\varepsilon = 0.0002$, [(c) and (g)] for $\varepsilon = 0.0045$, and [(d) and (h)] plotted for $\varepsilon = 0.001$.

conditions due to the coexistence of stable focus, saddle-node, and unstable focus equilibrium points inside the homoclinic orbit and an infinite number of nonisochronous periodic orbits outside this region. When one includes an external periodic force, the equilibrium points start moving back and forth depending on the forcing amplitude, and hence above the threshold value (F_c) the three-fixed-point system transformed into a single-fixed-point system and vice versa with respect to time. As a result, the dissipative and conservative regions oscillate in the time domain and therefore the dissipative region is expanded in the phase space. To verify this, in the autonomous Liénard system we have chosen an initial condition near to the homoclinic orbit (in the conservative region), and the resultant trajectory plotted in Fig. 3(a) shows that the system exhibits a neutrally stable periodic attractor. The chosen initial conditions are marked as black filled circles and the dissipative region is plotted as gray points. On the other hand, when we include the forcing with the magnitude $F = 0.2$ and for a suitable value of Ω, the periodic trajectory shown in Fig. 3(a) is now become unstable and evolved as chaotic orbit due to the expansion of the dissipative region which is depicted in Fig. 3(c). When the conservative and dissipative regions oscillate in terms of the external force, at some point of times, these two regions collide with each other near the saddle-node point. The chaotic trajectories crossing this saddle point are strongly repelled and make large excursions into the conservative region from its bounded motion, causing large-amplitude oscillations, and return to the chaotic orbit after a while. One such large excursion can be clearly seen in Fig. 3(c). If these excursions are frequent, then they are defined as MMOs. In contrast, rare and random excursions are characterized as extreme events. We point out here that the above-specified dynamical states arise only if we choose the initial conditions inside or near to the dissipative region. Nevertheless, when we choose the initial conditions further from the dissipative region, the autonomous Liénard system displays periodic motion as illustrated in Fig. 3(b) with the attractor larger than the orbit presented in Fig. 3(a) and in the presence of forcing the periodic orbit is now transformed into a quasiperiodic attractor. Figure 3(d) displays the emerged quasiperiodic attractor for $F = 0.2$.

IV. EFFECT OF TIME-DELAY FEEDBACK ON FORCED LIÉNARD SYSTEM

The primary objective of this paper is to understand the extreme event dynamics when including the self-time-delayed feedback. To this purpose, we have fixed the value of time delay $\tau = 0.1$ in Eq. (1) and vary the feedback strength (ε) to examine the effect of time delay on extreme events. Interestingly, we have identified that the large-amplitude chaotic bursts can be completely eliminated when increasing the feedback strength even for minimal values of ε. To verify this, we have plotted the dynamical variable y of Eq. (1) in Figs. 4(a)–4(d) and the corresponding phase portraits in Figs. 4(e)–4(h) for different values of ε. H_s is marked by a red (dark gray) horizontal line. In particular, in the absence of time delay ($\varepsilon = 0$), Fig. 4(a) exemplifies the occurrence of a thick band of bounded chaos along with intermittent large-amplitude chaotic bursts. Here these aperiodic intermittent random bursts occurred occasionally and were considerably larger than H_s. Hence they can be distinguished as extreme events. The phase portrait plotted in Fig. 4(b) also clearly

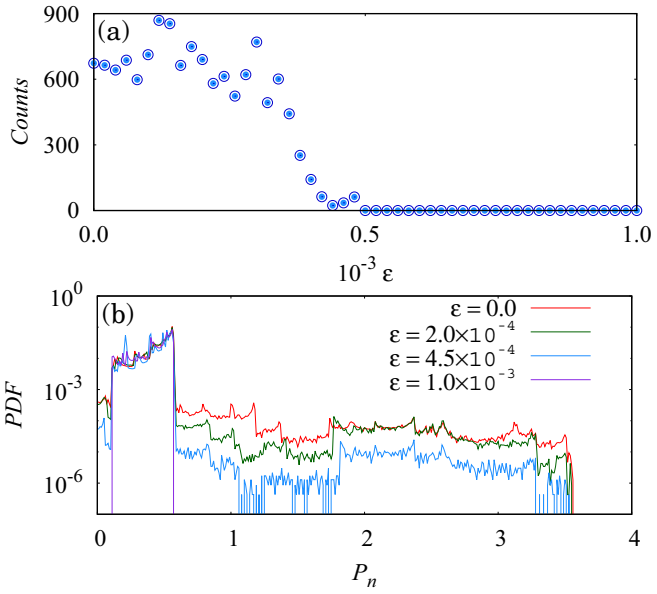

FIG. 5. (a) Number of extreme events as a function of the delay feedback strength (ε) and (b) the statistical distribution of the PDF for various values of ε.

indicates that the system exhibits a bounded chaotic orbit which is confined in a small part of the phase space (relatively) but rarely and aperiodically escapes from the orbit and displays large excursions and returns to the bounded chaotic orbit after some time. Figures 4(b) and 4(f), which are plotted for $\varepsilon = 0.0002$, show that the number of extreme events is reduced compared to the nondelayed case [Fig. 4(a)]. If we increase the feedback strength further to $\varepsilon = 0.0005$, then only a very few high-amplitude oscillations were observed, which is evident from Figs. 4(c) and 4(g). Finally, for $\varepsilon = 0.001$, the large-amplitude events are completely eliminated and only the bounded chaotic attractor is feasible [see Figs. 4(d) and 4(h)].

Therefore, when we increase the feedback strength, the number of extreme events are drastically reduced and eliminated for sufficient values of ε. Figure 5(a) is plotted between the number of events (peaks which are higher than H_s) versus feedback strength. For $\varepsilon < 0.00048$, the nonzero values of peak counts confirm the existence of extreme events and for $\varepsilon \approx 0.00048$, the number of events become zero corroborated that no extreme events occurred. In contrast, in Refs. [37,38], the authors reported that time-delayed feedback in an optical diode laser system with phase-conjugate feedback *induce* extreme events. In consequence, the number of high-amplitude pulses has been increased when increasing the feedback strength. Further, it has also been demonstrated that the probability of the occurrence of high-amplitude peaks transformed from Gaussian-shaped statistics to the long-tailed statistics (significant likelihood of extreme events) with increasing probability distribution when increasing the feedback strength (see Fig. 3 in Ref. [37]). But in our study, we have observed that the size (amplitude) of the extreme events remains almost equal and only the number of events get reduced when increasing the value of feedback strength. To verify this, we have further estimated the probability density function (PDF) of all the peaks for different values of feedback strength

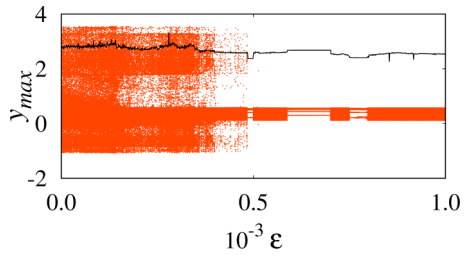

FIG. 6. One-parameter bifurcation diagram is drawn between the maxima of the dynamical variable y vs. feedback strength $\varepsilon \in (0.0, 1.0 \times 10^{-3})$ of Eq. (1) with $F = 0.2$, $\Omega = 0.7314$, and $\tau = 0.1$. The black line depicts H_s. Maxima appeared for $\varepsilon < 0.00048$ are larger than H_s corroborate the existence of extreme events.

and plotted it in a semilog scale [Fig. 5(b)]. Different color lines in the figure represent the PDFs for various ε values. From this figure, we can recognize that only the number of large-amplitude events decreased but the size of the extreme events is almost equal.

The bifurcation diagram plotted between maxima of the dynamical variable y versus feedback strength in the range of $\varepsilon \in (0.0, 0.001)$ is depicted in Fig. 6. The black line represents H_s. In the absence and for $\varepsilon < 0.00048$, the maxima of large-amplitude oscillations varies between $y_{\max} \in (-1.2, 3.6)$, and these amplitudes are higher than H_s, validating the occurrence of extreme events. After the critical value ($\varepsilon \approx 0.00048$), the large-amplitude events suddenly disappear and the system exhibits bounded chaotic oscillations. The global picture of the extreme event dynamics is studied and illustrated as a two-parameter diagram in Fig. 7 by varying the time delay (τ) and strength of the delay feedback (ε). Here the light yellow (gray) region represents the region where there is at least one peak larger than H_s (region of extreme events) and the red (dark gray) domain indicates nonextreme event region.

Accordingly, extreme events can be eradicated from the system dynamics when we add a self-delay feedback into the forced Liénard system. We also emphasize here that the

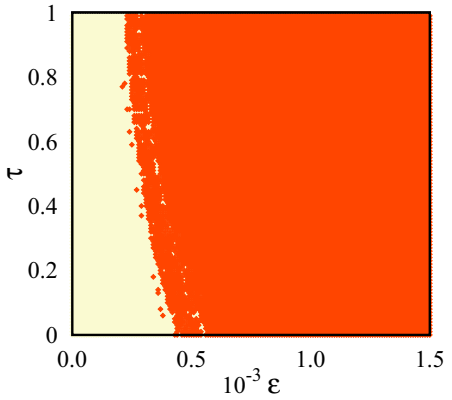

FIG. 7. Two-parameter diagram in the (ε, τ) plane of the forced Liénard system with delay feedback shows the occurrence of extreme event dynamics. Here the light yellow (gray) represents the region where extreme events occurred and the red (dark gray) domain is the nonextreme event region.

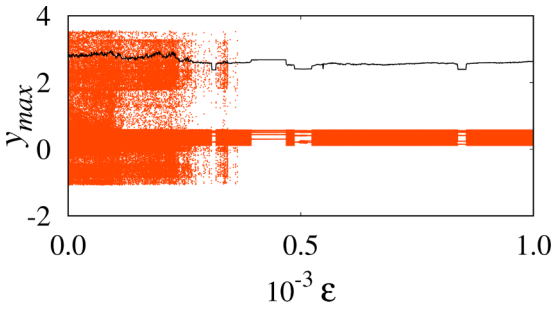

FIG. 8. Bifurcation diagram for the reduced equation [Eq. (6)] shows similar dynamical behavior as in Fig. 6. The black line depicts H_s as a function of ε.

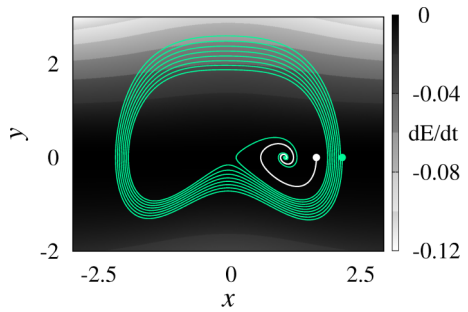

FIG. 9. Phase portrait of the autonomous Liénard system with delayed feedback with $\tau = 0.1$ and $\varepsilon = 0.08$. The rate of change of energy $\frac{dE}{dt}$ depicted as a gray-shaded region shows negative values, denoting that the system has a decaying solution in the whole phase space. The evolution of two trajectories that emerged from two different initial conditions (started inside and outside the homoclinic orbit) are illustrated in two different color lines. The chosen initial conditions are marked as filled circles.

MMOs can also eliminated from the system for appropriate values of time delay. More results are given in Appendix B.

A. Mechanism of controlling extreme events

We include the time delay in Eq. (1) with external force and rearrange it by considering the first two terms of the Taylor series expansion of the time-delay term $x_\tau = x(t) - \tau\dot{x}(t)$ as

$$\dot{x} = y, \tag{6a}$$

$$\dot{y} = -(\alpha x + \varepsilon\tau)y + (\gamma + \varepsilon)x - \beta x^3 + F\sin(\Omega t). \tag{6b}$$

The bifurcation diagram for Eq. (6) is plotted in Fig. 8 as a function of ε has a similar structure to that in Fig. 6, which was plotted for Eq. (1). The delay term $(\varepsilon\tau)$ in Eq. (6) contributes to the damping along with the (αx) term, confirming that time-delay feedback acts as a damping which destroys the conservative nature of the Liénard system and transforms the whole phase space as dissipative in nature. To confirm this, we have calculated the total energy of Eq. (6) without external forcing $(F = 0)$ and considering the $\varepsilon\tau y$ term as a perturbation which is given by

$$E = \frac{1}{2}\left\{y^2 + \frac{\alpha y}{2}\left[x^2 + \frac{(\gamma+\varepsilon)}{\beta}\right] + \frac{\beta}{2}\left[x^2 + \frac{(\gamma+\varepsilon)}{\beta}\right]^2\right\} \times e^{\frac{\alpha}{\omega}\tan^{-1}\left\{\frac{\alpha y + 2\beta\left[x^2 + \frac{(\gamma+\varepsilon)}{\beta}\right]}{2\omega y}\right\}} - \left[\frac{(\gamma+\varepsilon)^2}{4\beta}\right]e^{\frac{\alpha\pi}{2\omega}}, \tag{7}$$

and the rate of change of energy $(\frac{dE}{dt})$ of Eq. (7) can be written as

$$\frac{dE}{dt} = -e^{\frac{\alpha}{\omega}\tan^{-1}\left[\frac{\alpha y + 2\beta\left[x^2 + \frac{(\gamma+\varepsilon)}{\beta}\right]}{2\omega y}\right]} \times (\varepsilon\tau y). \tag{8}$$

The inequality $\frac{dE}{dt} < 0$ indicates that the system exhibits a decaying solution. When we add time-delay feedback to the system, the conservative nature disappears and only the dissipative nature remains in the entire phase space. As a result, the trajectories starting from anywhere in the phase space have an exponentially decaying solution and converge towards the stable focus at (1,0). To illustrate this, in Fig. 9 we have plotted the phase-space diagram of the two trajectories starting from two different regions (inside and outside the homoclinic orbit) for $F = 0$, $\tau = 0.1$ and fixed the feedback strength to $\varepsilon = 0.08$. The white trajectory in Fig. 9 is plotted for the initial condition chosen inside the homoclinic orbit which is converged to the stable focus faster than the nondelayed case. Nevertheless, initial conditions originated from outside of the homoclinic orbit [represented as green (light gray) trajectory] also slowly converged to reach the stable focus. However, for the nondelayed case these trajectories are neutrally stable periodic orbits, as shown in Fig. 1. We point out here that the trajectories with stronger feedback converge faster than the trajectories with weaker feedback strength. If we add the external force with suitable values of frequency (Ω) and amplitude (F), then the chaotic trajectory is evolved and confined in a small region of the phase space without having any large excursions. From these observations, one can understand that inclusion of time-delay feedback modified the system as dissipative in the whole phase space and acted as damping which destroyed the conservative nature of the Liénard system. We have also plotted the rate of change of energy $(\frac{dE}{dt})$ in Fig. 9 as a gray-shaded area that depicts that for the entire phase-space region $\frac{dE}{dt}$ obtain negative values, indicating the decaying solution. For $y = 0$, $\frac{dE}{dt} \approx 0$ corroborate that the trajectories reached the stable fixed point.

B. Anomalous damping

In general, during the damping, the amplitude of the oscillation decreases exponentially and becomes zero when $t \to \infty$. But it is interesting to note here that, in our study, we have revealed a type of damping phenomenon in a time-delayed autonomous Liénard system in which the amplitude of the oscillations is suddenly vanished when the total energy of the system becomes zero. We call this critical transition phenomenon *anomalous damping*. Figure 10 exemplifyies such a situation for two different initial conditions. In Fig. 10(a), we have plotted the time series of the trajectory started with the initial condition outside the homoclinic orbit which shows an exponentially decaying solution. This trajectory is expected to dampen as shown by the red (dark gray) dotted line. But suddenly the oscillations lose amplitude at a critical point of time (when the total energy $E = 0$) and reach the stable fixed point. The green (light gray) vertical line in Fig. 10(a) marks when $E = 0$. We have also plotted the rate of change of energy

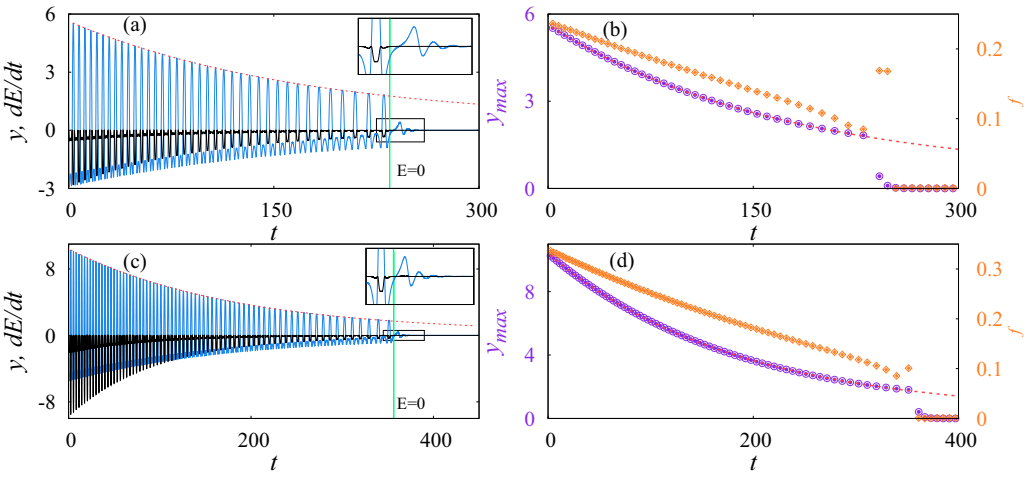

FIG. 10. [(a) and (c)] Time traces of the time-delayed autonomous Liénard system with $\tau = 0.1$ and $\varepsilon = 0.08$ for two different initial conditions showing anomalous damping behavior and [(b) and (d)] the corresponding amplitude and instantaneous frequency (f) of the system as a function of time.

$\frac{dE}{dt}$ (depicted as a black line), which shows negative values during damping and becomes zero when the oscillations reach the stable steady state [see inset of Fig. 10(a) for magnified image].

Further, we have already seen that these oscillations are nonisochronous outside the homoclinic orbit. Hence, during the damping process, the instantaneous frequency (f) is decreased and when $E = 0$ the trajectory produces fast oscillations (with increased frequency) to reach the stable point, which is also evident from Fig. 10(b). In this figure, the purple (dark gray) circles indicate the maxima of the y component of the system and the orange (light gray) points indicate the instantaneous frequency. Figures 10(c) and 10(d) depict similar types of anomalous damping behavior for different sets of initial conditions. We also emphasize here that one cannot attain anomalous damping when the initial conditions are chosen inside the homoclinic orbit.

V. CONCLUSION

To conclude, we have studied the dynamics of a Liénard-type system with and without external force and with time-delayed feedback. The autonomous Liénard system is capable of generating two distinct dynamical behaviors (dissipative and conservative) depending on the initial conditions. We have derived the expression for the total energy of the autonomous Liénard system which has null values in some region of phase space where the system exhibit dissipative dynamics. Nevertheless, if we choose the initial conditions outside this region, the system has an infinite number of coexisting neutrally stable periodic orbits which oscillate with respect to the saddle origin without losing their energy. This region is named as a conservative region in which the total energy has positive values. We have also identified that these periodic orbits are nonisochronous orbits where the instantaneous frequency increases if the amplitude of the oscillation increase.

We showed that under the influence of an external periodic force, the equilibrium points of the system oscillate along the x axis, which results from the transformation of a three-fixed-point system into a system with a single fixed point and vice versa. We found the exact timings when these transformations occurred. Because of the movement of the equilibrium points, the dissipative region enhanced in the phase space and collided with the conservative region at certain times near the saddle point. The trajectories of the bounded chaotic oscillations crossing the saddle point at these times will be repelled by the same and make large excursions in the phase space. When these large excursions happened frequently, they are MMOs and if these excursions are rare, then they are distinguished as extreme events. We have numerically explained the occurrence of MMOs and extreme events in a forced Liénard system using time series and bifurcation diagrams. Further, we have investigated the effect of self-time-delayed feedback on extreme events in this system and, interestingly, found that extreme events can be completely eliminated from the system dynamics even for smaller values of feedback strength. We proved that the number of extreme events is reduced with reference to the feedback strength by plotting the number of events versus feedback strength. We have also calculated the probability density function, which shows that the probability of the occurrence of high-amplitude peaks is transformed from a long-tailed statistics to the localized structure with respect to the feedback strength. The mechanism for the elimination of extreme events is examined with numerical evidence. We found that time-delay feedback acted as damping and destroys the conservative nature of the system. As a result, a dissipative nature alone is feasible in the entire phase space. Hence, the trajectories starting from the whole phase space only have a decaying solution, which is the reason and fundamental mechanism for the suppression of extreme events. Unlike the normal damping phenomenon, the decaying process we have observed here is interesting where the amplitude of the oscillations has suddenly vanished when the total energy of the system becomes zero, which we named anomalous damping. We also emphasize here that the results discussed in this paper are robust against the system and forcing parameter values. Since the Liénard system with time-delayed feedback is mimicking the optoelectronic laser

dynamical systems [57,58], the results demonstrated in this paper may also provide better knowledge about the dynamics, occurrence and the controlling aspects of the extreme events in such systems.

ACKNOWLEDGMENTS

The work of R.S. is supported by the SERB-DST Fast Track scheme for young scientists under Grant No. YSS/2015/001645. The work of V.K.C. forms part of a research project sponsored by the INSA Young Scientist Project under Grant No. SP/YSP/96/2014 and by the CSIR EMR Grant No. 03(1444)/18/EMR-II.

APPENDIX A: TEMPORAL DYNAMICS OF THE FORCED LIÉNARD SYSTEM

The bifurcation diagram in Fig. 2 shows the occurrence of different types of dynamical states in the forced Liénard system as a function of the forcing frequency. In particular, sudden changes in the amplitude of the system are observed and its temporal dynamical behavior is depicted in Figs. 11(a)–11(d) for different values of forcing frequency. Small-amplitude bounded chaos is evident from Fig. 11(a) for $\Omega = 0.7317$, and if we decrease the frequency value to $\Omega = 0.7314$ the system exhibit MMOs with rare and random occurrence of large-amplitude chaotic bursts as shown in Fig. 11(b). Hence this phenomenon is characterized as extreme events. The system exhibits MMOs with frequent large-amplitude chaotic bursts when we decrease the forcing frequency further. Figure 11(c) shows such frequent chaotic bursts for $\Omega = 0.7263$. We have chosen another Ω value near the intermittency region at $\Omega = 0.6423$ where the system exhibits extreme events, which is plotted in Fig. 11(d). There is a significant difference between Figs. 11(b) and 11(d) where in Fig. 11(b) the large chaotic bursts occurred randomly; nevertheless, in Fig. 11(d) the large chaotic bursts occurred almost at periodic intervals.

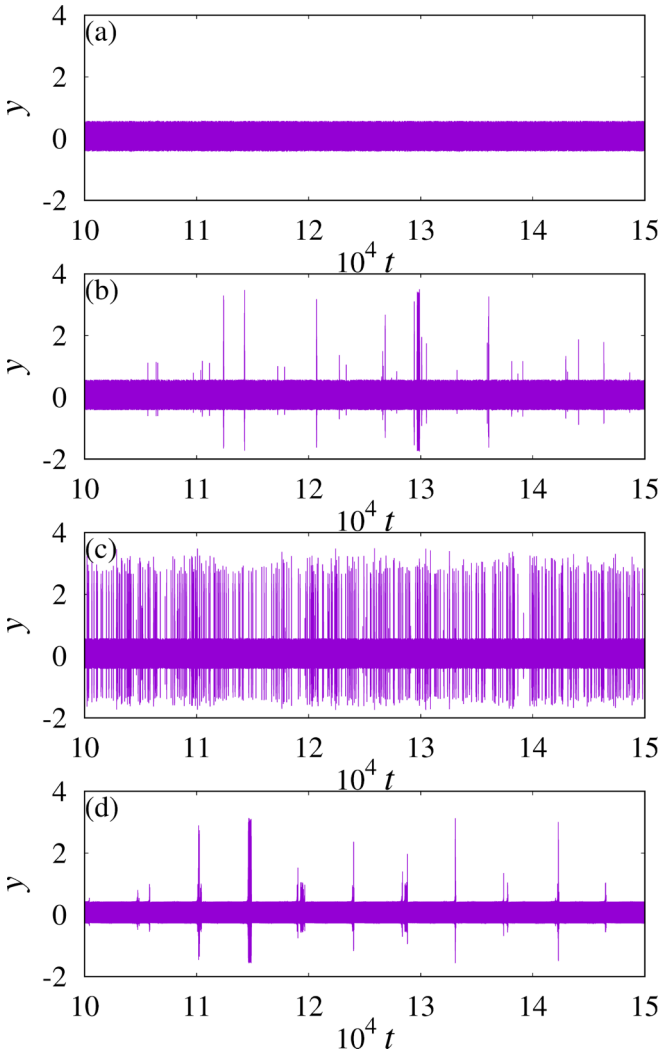

FIG. 11. [(a)–(d)] Temporal dynamics of the forced Liénard system with $F = 0.2$ and different values of forcing frequency (Ω). (a) For $\Omega = 0.7317$, (b) for $\Omega = 0.7314$, (c) for $\Omega = 0.7263$, and (d) is plotted for $\Omega = 0.6423$.

APPENDIX B: EFFECT OF TIME-DELAY FEEDBACK ON MMOS

It is evident from Fig. 2 that the forced Liénard system exhibits MMOs with large frequent chaotic bursts for the range of forcing frequency $\Omega \in (0.64225, 0.7316)$. We choose $\Omega = 0.7263$ and examine the effect of time-delay feedback on MMOs with frequent large-amplitude chaotic bursts, and the resultant outcomes are presented in Fig. 12. H_s is plotted

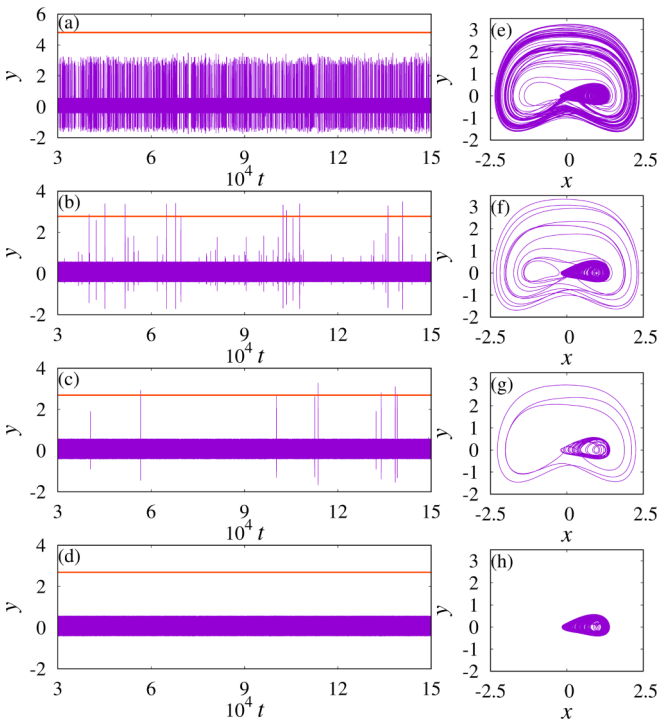

FIG. 12. [(a)–(d)] Temporal dynamics and [(e)–(h)] the corresponding phase-space diagrams of the forced Liénard system with $F = 0.2$, $\Omega = 0.7263$, $\tau = 0.1$ and for different values of the delay feedback strength (ε); [(a) and (e)] for $\varepsilon = 0.0$, [(b) and (f)] for $\varepsilon = 0.002$, [(c) and (g)] for $\varepsilon = 0.0023$, and [(d) and (h)] plotted for $\varepsilon = 0.0025$.

as a horizontal line to illustrate the rarity of the events. The occurrence of MMOs in the absence of delay feedback is represented in Fig. 12(a) as a temporal diagram where one can notice the frequent occurrence of large-amplitude chaotic bursts along with the bounded chaos. The corresponding phase portrait in Fig. 12(e) clearly shows the large excursions in the phase space. Here H_s is well above the maxima of the peaks, confirming that these peaks are not rare events. If we increase the strength of the delay feedback to $\varepsilon = 0.002$, then the number of events are drastically reduced and the recurrent phenomenon turns into rare events as shown in Figs. 12(b) and 12(f). The peaks above H_s confirm the occurrence of extreme events. If we increase the feedback strength further, then the number of large peaks furthermore decreases as described in Figs. 12(c) and 12(g) for $\varepsilon = 0.0023$. Finally, for $\varepsilon = 0.0025$ the large chaotic bursts can be completely removed from the system dynamics, and we obtain only small-amplitude bounded chaotic oscillations as depicted in Figs. 12(d) and 12(h) as time evolution and phase portrait plots, respectively.

Thus, we confirm that time-delay feedback can also capable of eliminating the MMOs with frequent large-amplitude chaotic bursts from the system for sufficient values of delay feedback strength. The results presented here are independent of the forcing frequency and amplitude.

[1] S. Albeverio, V. Jentsch, and H. Kantz, *Extreme Events in Nature and Society*, The Frontiers Collection (Springer, Berlin, 2006).

[2] K. Dysthe, H. E. Krogstad, and P. Müller, Annu. Rev. Fluid Mech. **40**, 287 (2008).

[3] M. A. Donelan and A.-K. Magnusson, Sci. Rep. **7**, 44124 (2017).

[4] A. Montina, U. Bortolozzo, S. Residori, and F. T. Arecchi, Phys. Rev. Lett. **103**, 173901 (2009).

[5] D. R. Solli, C. Ropers, P. Koonath, and B. Jalali, Nature **450**, 1054 (2007).

[6] C. Bonatto, M. Feyereisen, S. Barland, M. Giudici, C. Masoller, José R. Rios Leite, and J. R. Tredicce, Phys. Rev. Lett. **107**, 053901 (2011).

[7] S. Randoux and P. Suret, Opt. Lett. **37**, 500 (2012).

[8] M. Ghil *et al.*, Nonlin. Processes Geophys. **18**, 295 (2011).

[9] D. Sornette, *Critical Phenomena in Natural Sciences: Chaos, Fractals, Self-organization and Disorder: Concepts and Tools*, Springer Series in Synergetics (Springer, Berlin, 2003).

[10] L. Zhao, Y.-C. Lai, K. Park, and N. Ye, Phys. Rev. E **71**, 026125 (2005).

[11] P. Echenique, J. G. Gardeńes, and Y. Moreno, Europhys. Lett. **71**, 325 (2005).

[12] Y.-Z. Chen, Z.-G. Huang, H.-F. Zhang, D. Eisenberg, T. P. Seager, and Y.-C. Lai, Sci. Rep. **5**, 17277 (2015).

[13] K. Lehnertz, J. Biological Phys. **34**, 253 (2008).

[14] K. Lehnertz, Epilepsy: Extreme events in the human brain, in *Extreme Events in Nature and Society*, edited by S. Albeverio, V. Jentsch, and H. Kantz (Springer, Berlin, 2006), pp. 123–143.

[15] B. I. Jacobs, *Capital Ideas and Market Realities: Option Replication, Investor Behavior, and Stock Market Crashes* (Blackwell, Oxford, 1999).

[16] S. Bialonski, G. Ansmann, and H. Kantz, Phys. Rev. E **92**, 042910 (2015).

[17] S. Bialonski, D. A. Caron, J. Schloen, U. Feudel, H. Kantz, and S. D. Moorthi, J. Plankton Res. **38**, 1077 (2016).

[18] I. Dobson, B. A. Carreras, V. E. Lynch, and D. E. Newman, Chaos **17**, 026103 (2007).

[19] G. Ansmann, R. Karnatak, K. Lehnertz, and U. Feudel, Phys. Rev. E **88**, 052911 (2013).

[20] R. Karnatak, G. Ansmann, U. Feudel, and K. Lehnertz, Phys. Rev. E **90**, 022917 (2014).

[21] A. Saha and U. Feudel, Phys. Rev. E **95**, 062219 (2017); Chaos **28**, 033610 (2018).

[22] S. L. Kingston and K. Thamilmaran, Int. J. Bifurca. Chaos **27**, 1730025 (2017).

[23] S. L. Kingston, K. Thamilmaran, P. Pal, U. Feudel, and S. K. Dana, Phys. Rev. E **96**, 052204 (2017).

[24] P. P. Galuzio, R. L. Viana, and S. R. Lopes, Phys. Rev. E **89**, 040901 (2014).

[25] A. Rothkegel and K. Lehnertz, New J. Phys. **16**, 055006 (2014).

[26] M. G. Clerc, G. G. Cortés, and M. Wilson, Opt. Lett. **41**, 2711 (2016).

[27] W. Chang, J. M. S. Crespo, P. Vouzas, and N. Akhmediev, Opt. Lett. **40**, 2949 (2015).

[28] M. Farazmand and T. P. Sapsis, arXiv:1803.06277v1.

[29] J. Rinzel, A formal classification of bursting mechanisms in excitable systems, in *Mathematical Topics in Population Biology, Morphogenesis and Neurosciences* (Springer, Berlin, 1987).

[30] E. M. Izhikevich, Int. J. Bifurcat. Chaos **10**, 1171 (2000).

[31] J. Elezgaray and A. Arneodo, Phys. Rev. Lett. **68**, 714 (1992).

[32] M. Farazmand and T. P. Sapsis, Phys. Rev. E **94**, 032212 (2016).

[33] C. Van den Broeck, J. M. R. Parrondo, and R. Toral, Phys. Rev. Lett. **73**, 3395 (1994).

[34] A. B. Neiman and D. F. Russell, Phys. Rev. Lett. **88**, 138103 (2002).

[35] A. N. Pisarchik, R. Jaimes -Reátegui, R. Sevilla-Escoboza, G. Huerta-Cuellar, and M. Taki, Phys. Rev. Lett. **107**, 274101 (2011).

[36] J. A. Reinoso, J. Zamora-Munt, and C. Masoller, Phys. Rev. E **87**, 062913 (2013).

[37] A. K. Dal Bosco, D. Wolfersberger, and M. Sciamanna, Opt. Lett. **38**, 703 (2013).

[38] E. Mercier, A. Even, E. Mirisola, D. Wolfersberger, and M. Sciamanna, Phys. Rev. E **91**, 042914 (2015).

[39] V. H. Schultheiss, M. Wimmer, S. Malzer, and U. Peschel, Phys. Rev. X **8**, 011017 (2018).

[40] C. Lecaplain, Ph. Grelu, J. M. Soto-Crespo, and N. Akhmediev, Phys. Rev. Lett. **108**, 233901 (2012).

[41] H. L. D. de S. Cavalcante, M. Oriá, D. Sornette, E. Ott, and D. J. Gauthier, Phys. Rev. Lett. **111**, 198701 (2013).

[42] Y.-Z. Chen, Z.-G. Huang, and Y.-C. Lai, Sci. Rep. **4**, 6121 (2014).

[43] H. K. Joo, M. A. Mohamad, and T. P. Sapsis, Ocean Eng. **142**, 145 (2017).

[44] D. V. Ramana Reddy, A. Sen, and G. L. Johnston, Phys. Rev. Lett. **80**, 5109 (1998).
[45] U. Ernst, K. Pawelzik, and T. Geisel, Phys. Rev. E **57**, 2150 (1998).
[46] M. M. Shrii, D. V. Senthilkumar, and J. Kurths, Phys. Rev. E **85**, 057203 (2012).
[47] D. V. Senthilkumar, R. Suresh, J. H. Sheeba, M. Lakshmanan, and J. Kurths, Phys. Rev. E **84**, 066206 (2011).
[48] E. S. Medeiros, I. L. Caldas, M. S. Baptista, and U. Feudel, Nat. Sci. Rep. **7**, 42351 (2017).
[49] U. Feudel, A. N. Pisarchik, and K. Showalter, Chaos **28**, 033501 (2018).
[50] P. Ashwin, S. Wieczorek, R. Vitolo, and P. Cox, Philos. Trans. R. Soc. A **370**, 1166 (2012).
[51] G. C. McVittie, Mon. Not. R. Astron. Soc. **93**, 325 (1933); Y. P. Shah and P. C. Vaidya, Ann. Inst. H. Poincaré **6**, 219 (1967).
[52] P. G. L. Leach, J. Math. Phys. **26**, 2510 (1985).
[53] S. Chandrasekar, *An Introduction to the Study of Stellar Structure* (North-Holland, Amsterdam, 2006); J. M. Dixon and J. A. Tuszynski, Phys. Rev. A **41**, 4166 (1990).
[54] V. J. Erwin, W. F. Ames, and E. Adams, in *Wave Phenomena: Modern Theory and Applications*, edited by C. Rogers and J. B. Moodie (North-Holland, Amsterdam, 2006).
[55] S. Ghosh and D. S. Ray, Eur. Phys. J. B **87**, 65 (2014).
[56] C. N. Yang and R. L. Mills, Phys. Rev. **96**, 191 (1954).
[57] B. Romeira, J. Figueiredo, C. N. Ironside, and J. Javaloyes, Dynamics of Liénard optoelectronic oscillators, in *Selected Topics in Nonlinear Dynamics and Theoretical Electrical Engineering*, edited by K. Kyamakya, W. A. Halang, W. Mathis, J. C. Chedjou, and Z. Li (Springer-Verlag, Berlin, 2013), pp. 117–136.
[58] T. J. Slight, B. Romeira, L. Wang, J. Figueiredo, E. Wasige, and C. N. Ironside, IEEE J. Quant. Electron. **44**, 1158 (2008).
[59] F. M. Mahomed and P. G. L. Leach, Quaest. Math. **8**, 241 (1985); **12**, 121 (1989).
[60] L. G. S. Duarte, S. E. S. Duarte, and I. C. Moreira, J. Phys. A: Math. Gen. **20**, L701 (1987); S. E. Bouquet, M. R. Feix, and P. G. L. Leach, J. Math. Phys. **32**, 1480 (1991); W. Sarlet, F. M. Mahomed, and P. G. L. Leach, J. Phys. A: Math. Gen. **20**, 277 (1987); R. L. Lemmer and P. G. L. Leach, *ibid.* **26**, 5017 (1993); P. G. L. Leach, S. Cotsakis, and G. P. Flessas, J. Math. Anal. Appl. **251**, 587 (2000).
[61] V. K. Chandrasekar, M. Senthilvelan, and M. Lakshmanan, Proc. R. Soc. A **461**, 2451 (2005); Choas Solitons Fractals **26**, 1399 (2005).
[62] V. K. Chandrasekar, M. Senthilvelan, and M. Lakshmanan, Phys. Rev. E **72**, 066203 (2005).
[63] V. K. Chandrasekar, S. N. Pandey, M. Senthilvelan, and M. Lakshmanan, J. Math. Phys. **47**, 023508 (2006).
[64] R. L. Devaney, Trans. Am. Math. Soc. **218**, 89 (1976).
[65] A. Politi, G. L. Oppo, and R. Badii, Phys. Rev. A **33**, 4055 (1986).
[66] J. A. G. Roberts and G. R. W. Quispel, Phys. Rep. **216**, 63 (1992); J. S. W. Lamb, J. Phys. A **25**, 925 (1992); J. S. W. Lamb and J. A. G. Roberts, Physica D **112**, 1 (1998); H. W. Broer, I. Hoveijn, and M. van Noort, *ibid.* **112**, 50 (1998); H. Hanbmann, *ibid.* **112**, 81 (1998); B. Liu, Trans. Am. Math. Soc. **351**, 515 (1999).
[67] A. R. Champneys, Physica D **112**, 158 (1998).
[68] G. R. W. Quispel and J. A. G. Roberts, Phys. Lett. A **135**, 337 (1989).
[69] V. K. Chandrasekar, M. Senthilvelan, and M. Lakshmanan, J. Phys. A: Math Gen. **40**, 4717 (2007).
[70] V. C. Ruby, M. Senthilvelan, and M. Lakshmanan, J. Phys. A: Math. Theor. **45**, 382002 (2012).
[71] S. Karthiga, V. K. Chandrasekar, M. Senthilvelan, and M. Lakshmanan, Phys. Rev. A **93**, 012102 (2016).
[72] A. Mishra, C. Hens, M. Bose, P. K. Roy, and S. K. Dana, Phys. Rev. E **92**, 062920 (2015).
[73] M. Han and P. Yu, Fundamental theory of the Melnikov function method, in *Normal Forms, Melnikov Functions and Bifurcations of Limit Cycles* (Springer, London, 2012).